AN IMPRESSIVE RANGE of PRODUCTS

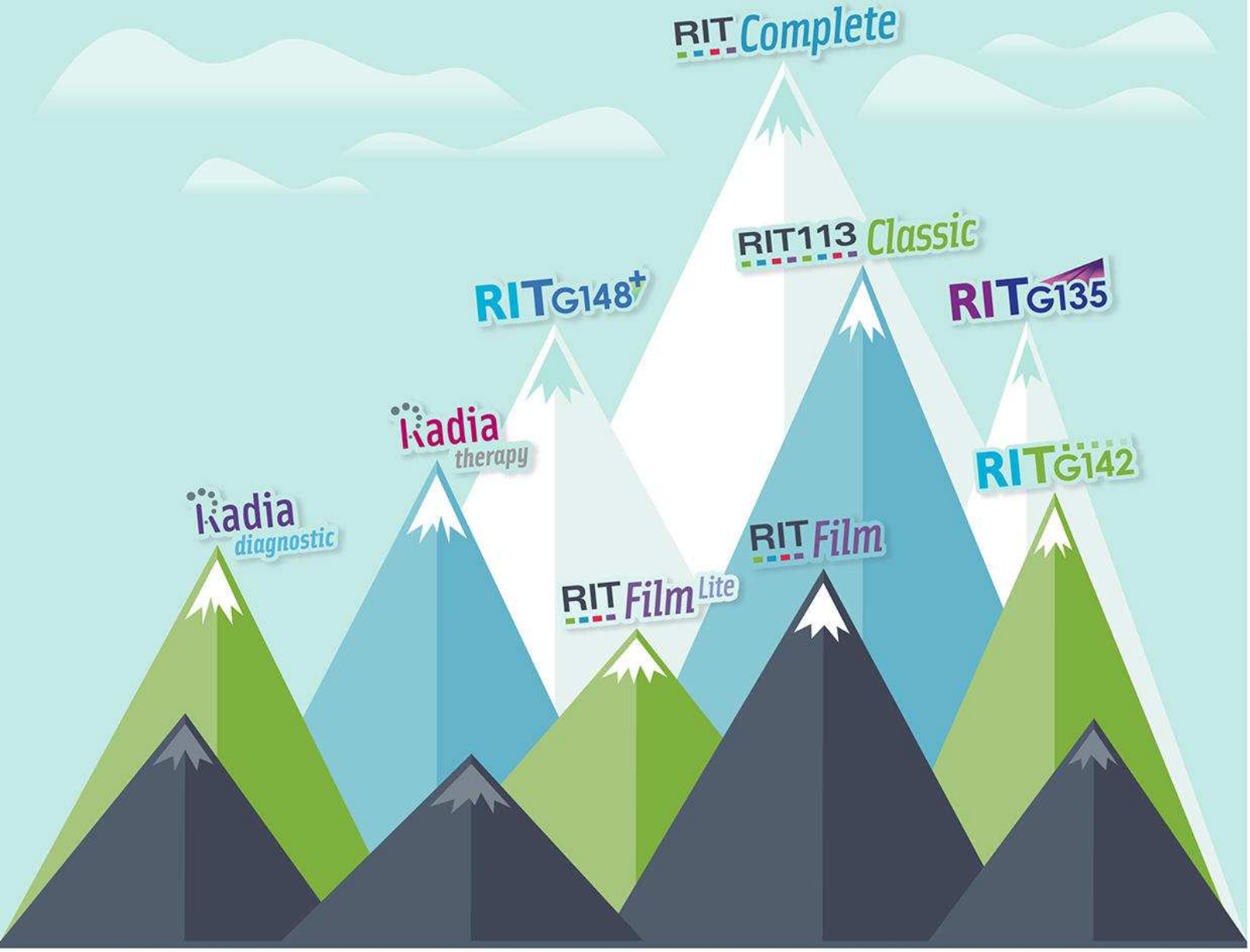

PATIENT QA | MACHINE QA | MLC QA | IMAGING QA

RIT

radimage.com

AT THE PEAK OF QA

Convenient packages that encompass basic testing to the most complete analyses in Medical Physics.

Connect with RIT

 | 719-590-1077 • sales@radimage.com | RIT is proudly headquartered in Colorado, at the base of Pikes Peak.

Calculating output factors for photon beam radiotherapy using a convolution/superposition method based on a dual source photon beam model

H. Helen Liu
Division of Radiation Oncology, Mayo Clinic and Foundation, Rochester, Minnesota 55905

T. Rock Mackie[a)]
Department of Medical Physics, University of Wisconsin, Madison, Wisconsin 53706

Edwin C. McCullough
Division of Radiation Oncology, Mayo Clinic and Foundation, Rochester, Minnesota 55905

(Received 9 January 1997; accepted for publication 1 October 1997)

A realistic photon beam model based on Monte Carlo simulation of clinical linear accelerators was implemented in a convolution/superposition dose calculation algorithm. A primary and an extra-focal sources were used in this beam model to represent the direct photons from the target and the scattered photons from other head structures, respectively. The effect of the finite size of the extra-focal source was modeled by a convolution of the source fluence distribution with the collimator aperture function. Relative photon output in air (S_c) and in phantom (S_{cp}) were computed using the convolution method with this new photon beam model. Our results showed that in a 10 MV photon beam, the S_c, S_p (phantom scatter factor), and S_{cp} factors increased by 11%, 10%, and 22%, respectively, as the field size changed from 3×3 cm^2 to 40×40 cm^2. The variation of the S_c factor was contributed mostly by an increase of the extra-focal radiation with field size. The radiation backscattered into the monitor chamber inside the accelerator head affected the S_c by about 2% in the same field range. The output factors in elongated fields, asymmetric fields, and blocked fields were also investigated in this study. Our results showed that if the effect of the backscattered radiation was taken into account, output factors in these treatment fields can be predicted accurately by our convolution algorithm using the dual source photon beam model. [S0094-2405(97)02412-7]

Key words: convolution/superposition, Monte Carlo simulation, extra-focal radiation, photon output factor, head scatter factor, phantom scatter factor, jaw exchange effect, asymmetric fields, multileaf collimator

I. INTRODUCTION

In radiation therapy, the absorbed dose delivered by a linear accelerator is calibrated in a reference field with a standard field geometry. To calculate dose for clinical treatments, the variation of the machine output from the reference field to the treatment field has to be taken into account. The secondary photons generated in the machine head were found to contribute most significantly to the changing of machine output with collimator opening.[1–7] This photon component was recently referred to as the ''extra-focal'' or the ''off-focus'' radiation.[4,5,7]

The photon output from the machine head is measured traditionally using an ionization chamber and a miniphantom positioned at the machine central axis. The dose scored in the miniphantom relative to that of a reference field (usually 10×10 cm^2 at SAD) has been defined as the ''collimator scatter factor'' [8] or S_c, although a name of ''head scatter factor'' could be used more appropriately. Another term S_{cp} is used to describe the relative photon output in a large water phantom. Its increase with field size is contributed by the head scatter S_c, and the phantom scatter S_p. Because the S_p can be difficult to measure directly, it is usually inferred by a ratio between the S_{cp} and S_c factors.

To calculate monitor units (MU) for a treatment field, MU of the calibrated field are converted using the above output factors to account for the change of the field geometries. Because the output factors are usually measured in simple fields along the central axis, more sophisticated treatment techniques, such as those using independent jaws, multileaf collimators (MLC), or specialized beam modifiers, have complicated the traditional way of calculating the MU. Measurements of the output factors for individual treatment geometries may be required occasionally. Therefore, a more automated and accurate method of MU calculation is more desired in the current clinical practice. Recently, convolution methods[7,9] have been used to model the output for photon fields. Sharpe *et al.*[7] estimated the effect of the extra-focal source from a measurement technique.[4] Ahnesjö *et al.*[9] calculated the photon output analytically by primarily accounting for the Compton scatter from the primary collimator and the flattening filter.

In our previous work, we have derived a dual source photon beam model based on Monte Carlo simulation of Varian 2100C linear accelerators.[10] In this work, we have investigated calculating the photon output factors using a convolution/superposition method[11–14] with this new photon

beam model. Based on the Monte Carlo data, we will demonstrate subsequently the effects of individual components in the machine head and the important contributing factors to the photon output. Thus the physical principles underlying various phenomena, such as the jaw exchange effects, the output in asymmetric fields and in blocked fields, can be well explained and unveiled. We will show that based on the new photon beam model, the convolution method can be used to predict the output factor for an arbitrary treatment field. This approach can be applied directly to calculate monitor units for patient treatments in an accurate and efficient manner.

II. MATERIALS AND METHODS

A. Monte Carlo simulation

Varian Clinac 2100C linear accelerators (Varian Oncology Systems, Palo Alto, CA) operated in photon 6, 10, and 18 MV modes were simulated using the Monte Carlo BEAM code.[15] The technical details of the simulation have been described in our previous work.[10]

Three types of open fields with jaws opened from 3 cm to 40 cm wide defined at SAD were simulated, including:

Square fields ''FSXY'' from 3×3 cm^2 to 40×40 cm^2;

Rectangular fields ''FSY'' defined by the Y jaws (upper jaws), which were opened from 3 cm to 40 cm apart, with the X jaws (lower jaws) fixed at 3 cm wide at SAD;

Rectangular fields ''FSX'' defined by the X jaws, which were opened from 3 cm to 40 cm apart, with the Y jaws fixed at 3 cm wide at SAD.

The photons reaching the scoring plane or the phase space plane below the jaws were separated into different components including the primary photons directly from the target, and the scattered photons (or the extra-focal photons) from other component modules. The energy fluence at the isocenter within a scoring region of 1.0 cm in diameter about the central axis, was recorded for each photon component in all the simulated fields.

The variation of the in-air photon output at different jaw settings is contributed by two factors: the change of energy fluence at the isocenter, and the change of monitor chamber scored dose due to the backscattered radiation from the jaws. From the scored energy fluence, the relative photon output (S_{ca}) was calculated as

$$S_{ca}(fs)=\frac{\Sigma_i\Psi_i(fs)}{\Psi_p(fs)}\Big/\frac{\Sigma_i\Psi_i(fs0)}{\Psi_p(fs0)}, \tag{1}$$

in which $\Psi_i(fs)$ is the energy fluence for the photon component i in the field size fs. The reference field size is $fs0$ (usually 10×10 cm^2 defined at SAD). The energy fluence from the primary photons $\Psi_p(fs)$, which was assumed to be invariant with field size, was used to normalize the total energy fluence at the isocenter for each field to reduce the statistical fluctuation of the simulation results.

From the monitor chamber scored dose, the relative photon output due to the backscattered radiation (S_{cb}) was calculated as

$$S_{cb}(fs)=\frac{Dc(fs)-Db(fs)}{Dc(fs)}\Big/\frac{Dc(fs0)-Db(fs0)}{Dc(fs0)}$$
$$=[1-Rb(fs)]/[1-Rb(fs0)], \tag{2}$$

in which $Dc(fs)$ and $Db(fs)$ are the dose scored in the monitor chamber in the total amount and from only the backscattered radiation, respectively, at field size fs. The ratio of $Db(fs)$ to $Dc(fs)$ was defined as the $Rb(fs)$ factor, i.e., the relative amount of the dose scored in the monitor chamber due to the backscattered radiation.

B. Convolution/superposition dose calculations

A collapsed cone based convolution/superposition dose calculation method was used in this study[11–14] to compute the photon output factors in air and in phantom. We have incorporated a new dual source photon beam model in this convolution algorithm.[10] Two photon sources were used in the beam model: a primary photon source for the direct photons from the target, and an extra-focal photon source for the scattered photons mostly from the flattening filter and the primary collimator. The fluence and spectral distributions of the two photon sources, as well as their geometrical distributions were used by the convolution algorithm to compute terma and dose distributions. In particular, the extra-focal photon fluence was modeled by convolving the source distribution with the collimator aperture function defining the field size.[10] The primary source was approximated by an ideal point source, whose fluence at the isocenter was assumed to be constant and was used to normalize the total terma and dose from the convolution calculation.

1. Relative photon output in air

Using a method similar to the method used for the Monte Carlo phase space data, the relative output in air was calculated from the energy fluence as

$$S_{ca}(fs)=\frac{\Psi_p(fs)+\Psi_s(fs)}{\Psi_p(fs0)+\Psi_s(fs0)}, \tag{3}$$

in which $\Psi_p(fs)$ and $\Psi_s(fs)$ are the calculated energy fluence from the primary source and the extra-focal source, respectively, at the center of the field fs. In the convolution calculation, $\Psi_p(fs)$ is constant in all the fields, while $\Psi_s(fs)$ increases with field size. The S_{ca} factors calculated by the convolution method were verified by the Monte Carlo data [Eq. (1)].

According to the traditional way of measuring the photon output in air, we also computed dose in a simulated miniphantom using the convolution method. The phantom was placed at 100 cm SSD with a dimension of 3×3 cm^2 in cross section and 7 cm in length along the machine central axis direction. The head scatter factor $S_{ca}(fs)$ was also calculated as

$$S_{ca}(fs)=D(fs)/D(fs0), \tag{4}$$

in which $D(fs)$ is the calculated dose at a depth of 5 cm along the central axis in the miniphantom. Because the dual

source photon beam model was used, the dose was contributed from both the primary and the extra-focal sources.

To account for the reducing of the backscattered radiation to the monitor chamber, the total photon output in the miniphantom was calculated as

$$S_c(fs) = S_{ca}(fs) \times S_{cb}(fs), \tag{5}$$

in which $S_{cb}(fs)$ is from the Monte Carlo simulation [Eq. (2)]. Thus the backscatter corrected head scatter factors were able to be compared to the measured data directly.

We have computed the S_{ca} and S_c factors for the three types of fields ''FSX,'' ''FSY,'' and ''FSXY.'' These factors were compared to those from the Monte Carlo results and the measured data. To study the effects of SSD and depth on the head scatter factor, S_{ca} was computed for symmetric fields $3\times3-40\times40$ cm^2 (defined at SAD) at 80–150 cm SSD. At 100 cm SSD, S_{ca} was also computed 0.5 cm–10 cm deep within the miniphantom with the phantom length varied from 7 cm to 12 cm.

2. Phantom scatter factors

The phantom scatter factors S_p were calculated using the convolution method as

$$S_p(fs) = D_p(fs)/D_p(fs0), \tag{6}$$

in which $D_p(fs)$ is the dose calculated using only the primary photon source, as its fluence does not change with field size. Thus only the scatter within the phantom contributes to the S_p factor. Dose was calculated 5 cm deep in a water phantom with a dimension of $50\times50\times50$ cm^3. Symmetric fields of $3\times3-40\times40$ cm^2 of 6, 10, and 18 MV photon beams were used for the S_p calculation.

3. Total output factors in phantom

The total output factors in phantom S_{cp} were computed similarly to S_p except both the primary and the extra-focal sources were used in the calculation. We have also computed S_{cp} alternatively as a product of the S_c and S_p factors[8] calculated by the convolution method. To compare the calculated S_{cp} with the measured data, the S_{cb} factors from the Monte Carlo data were used similarly to Eq. (5) to correct for the backscatter effect. S_{cp} were calculated for symmetric fields of $3\times3-40\times40$ cm^2. We also computed S_{cp} in asymmetric fields of $3\times3-30\times30$ cm^2. The fields were centered at 5 cm off-axis along both x and y directions on the isocenter plane. The dose was calculated 5 cm deep in the water phantom at $(x,y)=(5,5)$ cm in the asymmetric fields.

To model the output factors in the fields shaped by a multileaf collimator, we have implemented a Varian 40 leaf collimator module in the convolution algorithm. This implementation did not involve any additional Monte Carlo simulation of the MLC. The specifications of the MLC in our convolution algorithm included the position of each leaf end projected at 100 cm SAD as well as the z axis location of the leaf aperture. The dose distribution calculated in the MLC fields, particularly in the penumbra regions and outside the beams due to the leaf leakage were verified by the dose profiles measured in a water phantom using a Wellhöfer scan system (Wellhöfer Dosimetrie, Nürnberg, Germany) with an IC10 chamber (0.147 cc collection volume). Using the convolution algorithm, we computed dose 5 cm deep along the central axis in the water phantom for the MLC defined fields. The relative output in the water phantom was computed using the reference field of 10×10 cm^2 defined by the MLC at 100 cm SAD.

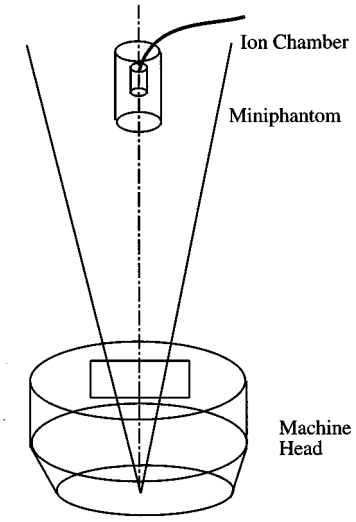

FIG. 1. Illustration of the measurement for the head scatter factor (not in a realistic scale). The gantry angle is 180 degree. A Wellhöfer chamber was placed 5 cm deep from the front surface of the miniphantom, which is 3 cm in diameter and 7 cm in length.

C. Measurements

1. Head scatter factors

The head scatter factors were measured in air using a cylindrical miniphantom of water (Fig. 1). It had a dimension of 3 cm in diameter and 7 cm in length. The phantom was placed at 100 cm SSD coaxially with the machine central axis. The Wellhöfer IC10 chamber was placed in the miniphantom 5 cm deep from the front surface of the phantom (105 cm source to chamber distance). The chamber was also coaxial with the machine central axis. A measurement depth of 5 cm was chosen to avoid electron contamination in the beam.[16] The charge $Q(fs)$ collected by the ion chamber per 100 MU was recorded for each field with field size fs. For a rectangular field ''FSX'' or ''FSY,'' the average charge reading was taken from those of the collimator rotation angles of 0, 45, and 90 degrees. The in-air output factor $S_c(fs)$ was computed as

$$S_c(fs) = \frac{Q(fs)}{Q(fs0)}. \tag{7}$$

$Q(fs)$ was measured for the three types of fields ''FSX,'' ''FSY,'' and ''FSXY'' at 6, 10, and 18 MV photon energies on the Clinac 2100C machines.

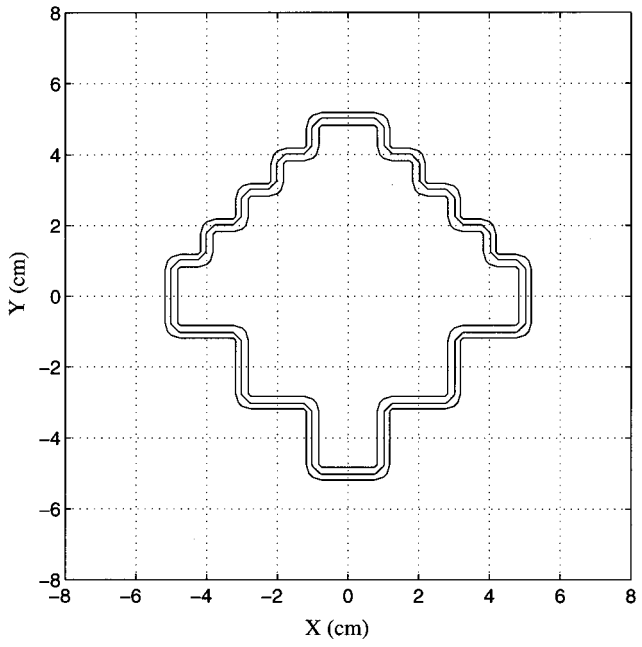

FIG. 2. The mushroom shaped field defined by the MLC with 10 pairs of leaves open and 10 cm in field width. The leaf motion direction is along the x axis.

2. Total output factors in phantom

The total output factors S_{cp} were also measured using the Wellhöfer IC10 chamber within a large water phantom with a dimension of $60\times60\times60\ \text{cm}^3$ approximately. The phantom was placed at 100 cm SSD. The chamber was immersed 5 cm deep in the phantom at the center of the fields. The S_{cp} was calculated in the same way as the S_c [Eq. (7)] except that the measured data were taken within the large water phantom. The S_{cp} was measured for the ''FSXY'' square fields, and asymmetric fields of $3\times3-30\times30\ \text{cm}^2$ centered at 5 cm off-axis along both x and y directions. For the asymmetric fields, the chamber was also placed at the center of the field 5 cm deep within the phantom. In order to avoid the effect of beam asymmetry, the average reading from four possible jaw settings were taken, i.e., with the asymmetric fields centered at $(x,y)=(5,5),(-5,5),(5,-5)$, and $(-5,-5)$ cm.

The relative output factors in the MLC fields were measured along the machine central axis 5 cm deep by the Wellhöfer IC10 chamber in the water phantom. The measurements were taken in the fields including a set of square fields $4\times4-28\times28\ \text{cm}^2$, a set of mushroom shaped fields using 4–14 pairs of leaves (Fig. 2), and clinical treatment fields with irregular shapes. These fields were defined solely by the MLC. The jaws were kept at $35\times35\ \text{cm}^2$ wide apart at SAD in any fields. In this case, the backscattered radiation from the jaws did not affect the relative output. Yet because the leaves were rounded at the edge, the leakage through the leaf ends when they were fully closed left a gap about 1–2 mm in width at SAD. This gap was perpendicular to the leaf motion direction and was not blocked by the jaws. This leakage was approximated by a 1 mm wide opening in our convolution calculation, as the leakage contribution to the center of the small fields was found to be significant. The relative output in the MLC defined field was calculated from the measured chamber collected charge. The reference field was chosen to be the $10\times10\ \text{cm}^2$ field at SAD defined by the MLC rather than by the jaws in order to avoid the complication from the backscattered radiation.

3. Backscattered radiation to the monitor chamber

The effect of the backscattered radiation from the jaws to the monitor chamber was measured using the technique described previously by Sharpe *et al.*[7] This method assumes that the photon output is linearly proportional to the number of electron pulses hitting the target provided that the number of electrons per pulse is relatively stable. The monitor chamber collected charge, which should be constant for the same MU setting, determines the number of output electron pulses in a radiation field. The chamber collected charge is contributed by both the forward radiation and the backscattered radiation mostly from the jaws. Thus the effect of the backscattered radiation is estimated from the number of electron pulses at different jaw settings.

The signal of the electron pulse hitting the target was taken from the control console of a Clinac 2100C machine. This signal was processed by a pulse generation circuit to output positive ($+5$ V) and short duration pulses (0.5 μs) corresponding to each electron pulse. The circuit contained two stage operational amplifiers (μA741) and a short pulse generator (DM74LS123). The output signal was input to a multi-channel analyzer (Canberra 35 Plus) to count the number of electron pulses. The measurements were taken at multiple times and at different MU settings (50–250 MU) for each field to obtain linear and stable readings.

The number of pulses per 100 MU at each field size, $NP(fs)$, was used to estimate the output increase due to the backscattered radiation alone. Similar to the analysis used for the Monte Carlo simulation data, the head scatter factor S_c [Eq. (7)] can be broken down into two parts:

$$S_c(fs)=\left[\frac{Q(fs)}{NP(fs)}\Big/\frac{Q(fs0)}{NP(fs0)}\right]\times\left[\frac{NP(fs)}{NP(fs0)}\right], \tag{8}$$

in which $Q(fs)$ is the Wellhöfer chamber collected charge in the miniphantom for field size fs. The fraction terms in the first and the second pairs of brackets of Eq. (8) can be treated as the $S_{ca}(fs)$ and the $S_{cb}(fs)$ factors, respectively. They reflect the effects of the photon energy fluence and the backscattered radiation, respectively, on the change of photon output in air.

The number of pulses per 100 MU was measured for the fields of $3\times3\ \text{cm}^2-40\times40\ \text{cm}^2$ at the 6, 10, and 18 MV photon energies on the Varian 2100C machines. The $S_{cb}(fs)$ factor computed as the relative pulse number $NP(fs)/NP(fs0)$ was compared to the Monte Carlo data [Eq. (2)].

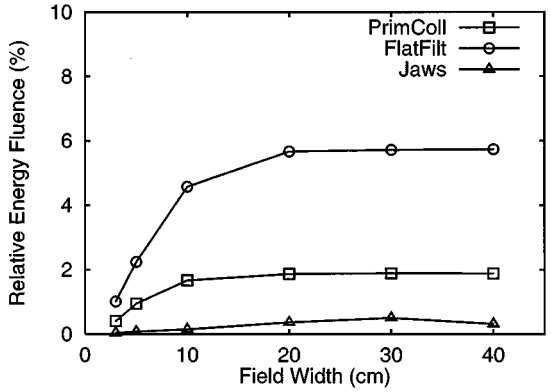

FIG. 3. The relative photon energy fluence (normalized to that of the primary photons) of the three scattered photon components as a function of field size (square fields). The results are based on the Monte Carlo phase space data of the 10 MV photon beam. ''PrimColl,'' ''FlatFilt,'' and ''Jaws'' are of photons scattered from the primary collimator, the flattening filter, and the jaws, respectively.

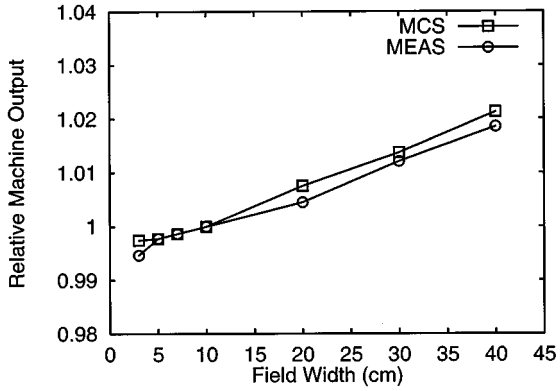

FIG. 5. The head scatter factors due to the reduction of the backscattered radiation into the monitor chamber (S_{cb}) as a function of field size (square fields). Results are from the Monte Carlo simulation (''MCS'') and the measurement (''MEAS''). The data are of the 10 MV photon beam.

III. RESULTS AND DISCUSSION

A. Relative photon output in air

Figure 3 shows the relative energy fluence (normalized to that of the primary photons) from the three scattered photon components at the isocenter of the 10 MV photon beam. The results are obtained from the Monte Carlo phase space data. The field sizes are 3×3 cm^2–40×40 cm^2. Figure 3 shows that the energy fluence of the scattered photons from the primary collimator, the flattening filter, and the jaws increases with the field size. The flattening filter and the primary collimator contribute the majority of the extra-focal photons, while the jaws have little effect on the total energy fluence of the scattered photons. The increase of the extra-focal photons with field size is caused by the large source size of the extra-focal photons. Thus the jaws act as an aperture window on the extra-focal source, limiting the number of scattered photons reaching the scoring plane. This effect has been modeled in our convolution algorithm by a convolution of the source distribution with the jaw aperture function.[10,17,18]

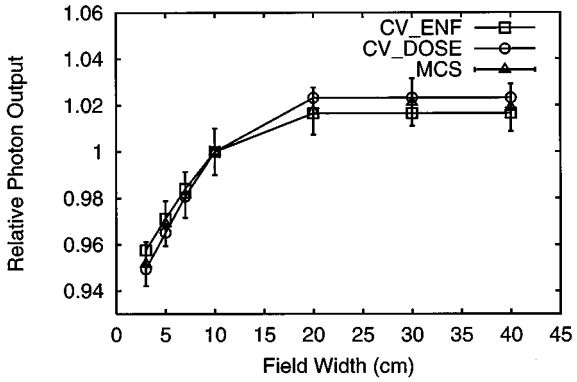

FIG. 4. The relative photon output in air calculated from the energy fluence using the convolution method (''CV_ENF'') and the Monte Carlo simulation (''MCS''). The in-air output factors calculated from the dose in the miniphantom using the convolution method are shown by ''CV_DOSE.'' The data are of the 10 MV photon beam.

Figure 4 shows the relative photon output measured by the total energy fluence at the isocenter from the Monte Carlo data [Eq. (1)], and the two convolution calculation methods: data of ''CV_ENF'' are based on the energy fluence [Eq. (3)]; data of ''CV_DOSE'' are based on the calculated dose [Eq. (4)]. The 10×10 cm^2 field defined by the jaws is the reference field. The results from the Monte Carlo simulation (''MCS'') and the convolution calculation (''CV_ENF'') using the energy fluence agree within 2% for all the fields. This shows that the convolution approach, which uses the photon beam model based on the phase space data, can reproduce the variation of the extra-focal photons accurately in different fields.

The results also show that the S_{ca} factors calculated from the dose scored in the miniphantom (''CV_DOSE'') are about 1.0% different than the S_{ca} calculated from the energy fluence (''CV_ENF''). This is because the dose is not only related to the energy fluence, but also depends on the local energy deposition and the phantom scatter within the miniphantom. In other words, the dose based S_{ca} is a phantom dependent factor, which could vary slightly from the S_{ca} factor exclusively based on the energy fluence output from the machine head. Figures 3 and 4 also show that the photon output increases more significantly in smaller fields from 3×3 to 10×10 cm^2 than in larger fields from 20×20 cm^2 to 40×40 cm^2. This is because in the small fields the extra-focal source is partially eclipsed by the jaws, while in larger fields the majority of the extra-focal source has been exposed. Thus the extra-focal photon fluence is relatively stable beyond the 20×20 cm^2 field.

B. Backscattered radiation to the monitor chamber

Figure 5 shows the S_{cb} factors (relative photon output due to the backscattered radiation alone) in the fields of 3×3 -40×40 cm^2 of the 10 MV photon beam. Equation (2) was used to calculate the $S_{cb}(fs)$ from the Monte Carlo simula-

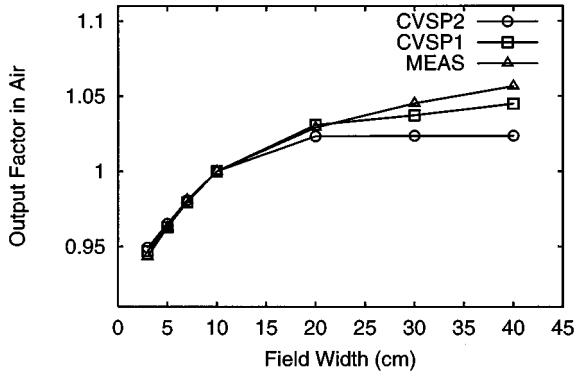

FIG. 6. The head scatter factors S_c from the convolution calculation with and without the backscatter correction (''CV_BK'' and ''CV,'' respectively), and from the measurement (''MEAS''). The data are of the 10 MV photon beam.

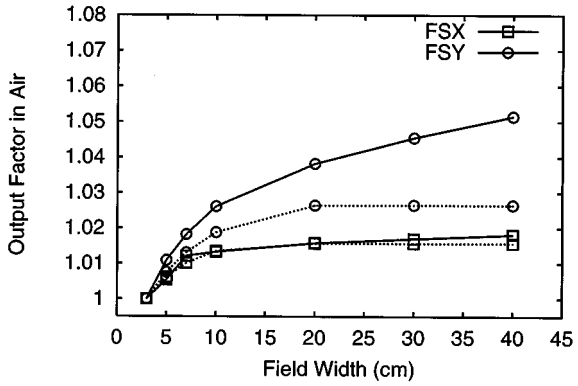

FIG. 7. The head scatter factors in the rectangular ''FSX'' and ''FSY'' fields from the measurement (solid lines), and the convolution calculation (S_{ca}, dotted lines). The backscatter correction is not included in the convolution calculation. The data are of the 10 MV photon beam.

tion data. The one standard deviation of this S_{cb} increases from 1% in the field of 3×3 cm^2 to 2% in the field of 40 $\times40$ cm^2. The relative pulse count $NP(fs)/NP(fs0)$ was used to calculate the $S_{cb}(fs)$ from the measured electron pulses. The one standard deviation of this $S_{cb}(fs)$ is 1%–2% for all the fields. The kapton monitor chamber was used in the Monte Carlo simulation and the measurements. Both set of data show that the reduced backscattered radiation contributes about 2% to the increase of the photon output. The results of the 6 MV and the 18 MV beams indicated a similar effect of the backscattered radiation. The data agree with the previously published results of Varian machines.[19] In general, most studies have estimated the backscattered radiation caused the output to increase within 0.5%–4.0%, based on different techniques on various treatment machines.[7,20–23]

Our Monte Carlo data also indicated that the relative dose scored from the backscattered radiation $Rb(fs)$ factor [Eq. (2)] decreased from 5% in the field of 3×3 cm^2 to 3% in the field of 40×40 cm^2. The backscattered radiation was contributed mostly by the scattered electrons and lower energy photons from the upper jaws. They could be partially eliminated by either increasing the distance from the monitor chamber to the jaws, or by using more attenuating window material for the lower surface of the chamber. For example, our Monte Carlo simulation showed that the $Rb(fs)$ factor was reduced to about 0.5%–1.0% for a mica chamber which uses aluminum as the exit window and the separation sheets. Thus the jaw position had little effect on the mica chamber scored dose. This is obviously more desirable for an accurate modeling of the relative photon output using a model based dose calculation method such as the convolution method.

C. Head scatter factors in square fields

Figure 6 shows the S_c factors in the square fields of the 10 MV photon beam. The results from the convolution calculation with and without the backscatter correction [Eqs. (4) and (5)] are compared to the measured data. The figure shows that the measured and the calculated S_c agree relatively well, particularly in small fields. In the larger fields, the calculated S_{ca} factor remains flat beyond the field of 20×20 cm^2 because the majority of the source has been exposed. The measured data continue to increase about 2% more, which can be accounted for by using the backscatter correction. In our photon beam model, the scattered photons from the flattening filter were only used to represent the distribution of the extra-focal source.[10] Thus the scattered photons from the other component modules may not be modeled exactly by the extra-focal source. This could have caused about 1% underestimation of the S_c factors compared to the measured data in the largest fields.

Figures 4, 5, and 6 show that the photon output in air increases about 11% from the field of 3×3 cm^2 to the field of 40×40 cm^2. Of this amount of increase, 9% is contributed by an increase of the extra-focal photon fluence, and 2% is contributed by a reduction of the backscattered radiation. Our results indicated that the S_c increase was about 10% for the 6 MV beam, and 11% for the 18 MV beam in the same field range. The variation of the S_c factor does not change significantly with the beam energy, because the intensity of the extra-focal source compared to the primary source is not strongly affected by the photon energy.[10]

D. Jaw exchange effect

Figure 7 shows the in-air output factors from the measurement and from the convolution calculation (without the backscatter correction) in two types of rectangular fields ''FSX'' and ''FXY'' of the 10 MV photon beam. The 3 $\times3$ cm^2 field is used as the reference field. The measured data show that the S_c is about 3% higher in the ''FSY'' field than in the ''FSX'' field at the largest field width. This jaw exchange effect is caused by both the backscatter effect and the finite size of the extra-focal source.

1. Backscatter effect

As the Y jaws are closer to the monitor chamber, the amount of the backscattered radiation varies more significantly with the Y jaw movement than with the X jaw movement. Thus the effect of the backscatter is more prominent in the ''FSY'' fields than in the ''FSX'' fields, because in the later case, the Y jaws are consistently closed at 3 cm apart (at

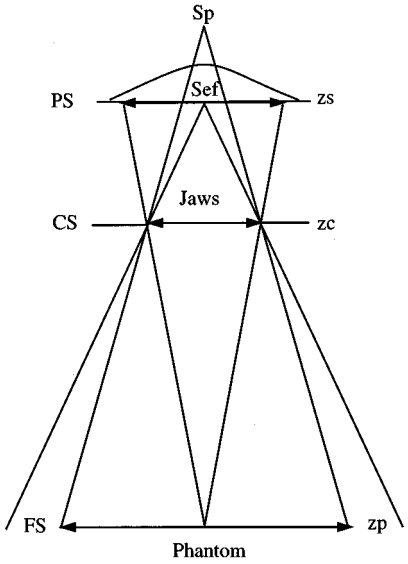

FIG. 8. Illustration of the dual source photon beam geometry. The primary photon source is Sp and the extra-focal source is Sef. The locations of the extra-focal source, the jaws and the phantom are zs, zc, and zp, respectively, along the central axis. The field size is FS, which corresponds to the jaw opening CS, and the projection of the jaws PS on the extra-focal source.

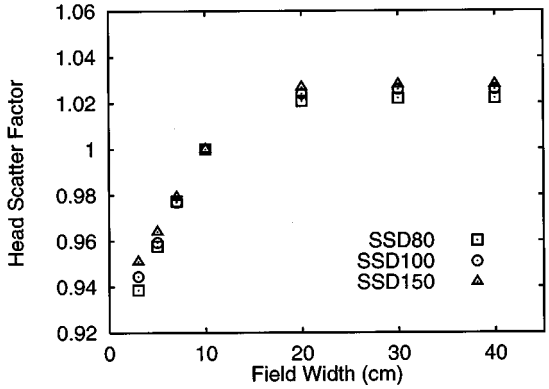

FIG. 9. The head scatter factors from the convolution calculation as a function of field size (defined at SAD) for the phantom SSD of 80 cm (''SSD80''), 100 cm (''SSD100''), and 150 cm (''SSD150''). The data are of the 10 MV photon beam.

SAD). Our Monte Carlo simulation data showed that the magnitude of the relative backscattered dose $Rb(fs)$ in the ''FSX'' fields did not change significantly with the field width, while the $Rb(fs)$ in the ''FSY'' fields were compa rable to those in the ''FSXY'' (square) fields. The difference between the the measured S_c and the calculated S_{ca} ranges from 0.8% to 2.3% in the ''FSY'' fields with the field width increased from 10 cm to 40 cm. This agrees well with the $S_{cb}(fs)$ from the Monte Carlo and measured data. The S_c factor in the ''FSX'' fields, which is not significantly affected by the backscattered radiation, was predicted more accurately by the convolution calculation, shown by the results.

2. Jaw aperture effect on the extra-focal source

Figure 7 also shows that the photon output calculated by the convultion approach is about 1.0% higher in the ''FSY'' fields than in the ''FSX'' fields at larger field width. This is because the amount of the extra-focal radiation reaching the phantom also depends on the location of the aperture used to define the field. This is illustrated by Fig. 8. In this figure, the primary source and the extra-focal source are represented by ''Sp'' and ''Sef,'' respectively. The z axis (machine central axis) positions of the extra-focal source, the simplified aperture of X or Y jaws, and the scoring plane are zs, zc and zp, respectively. The field size FS corresponds to the jaw opening of CS. The projection of the jaws on the extra-focal source plane at zs (from the field center at zp) is PS, which can be found by

$$PS = CS \times \frac{zp - zs}{zp - zc}$$

$$= FS \times \frac{zc}{zp} \times \frac{zp - zs}{zp - zc}. \quad (9)$$

For both the X and Y jaw defined fields, FS, zp and zs are the same, yet zc of the X and Y jaws (upper level of the jaws) are about 37 cm and 28 cm, respectively, on the Clinac 2100C machine. This causes the PS from the X jaws larger than that of the Y jaws for the same FS defined on the isocenter plane. For example, for both jaws to be opened at 3 cm wide on the 100 cm SSD plane, the PS for the X and Y jaws on the extra-focal source plane are 1.60 cm and 1.06 cm, respectively ($FS = 3$ cm, $zp = 100$ cm, $zs = 9.5$ cm, data from our previous study[10]). The larger projection size from the X jaws, or in other words, the larger exposed area of the extra-focal source seen through the X jaws, will allow more scattered photons to reach the scoring plane. This causes the S_{ca} factors of the largest ''FSY'' fields with the X jaws fixed at 3 cm apart to be greater than those of the largest ''FSX'' fields with the Y jaws fixed at 3 cm apart. The results have been demonstrated by the convolution calculation.

The combined effects of the backscattered radiation and the finite source size cause the difference in the photon output for the elongated fields with alternative jaw settings. Previous studies[24–26] have reported similar results. In addition, if blocks or MLC are used to define the field size instead of the jaws, the difference in photon output also occurs,[26–28] because these beam modifiers are further away from the source than the X jaws. This will be discussed in more detail in the subsequent section.

E. SSD and depth dependence of head scatter factors

Gasteren *et al.*[16] have suggested that the in-air output factors are independent of the measurement SSD or depth in a miniphantom. Thus the S_c of small fields can be measured at an extended distance to provide a lateral electron equilibrium. To evaluate this conclusion, we calculated the S_{ca} factors at different phantom SSDs and depths within the

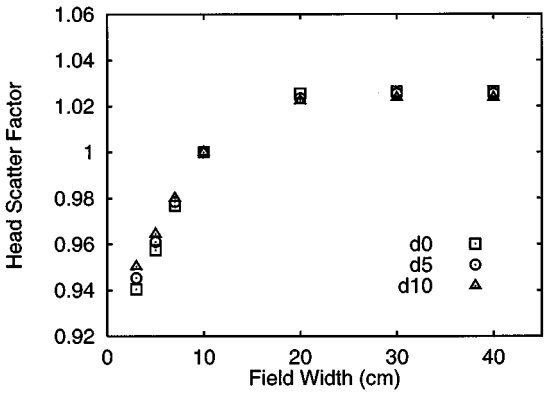

FIG. 10. The head scatter factors from the convolution calculation as a function of field size for the calculation depths of 0.5 cm (''$d0$''), 5 cm (''$d5$''), and 10 cm (''$d10$''). The phantom is at 100 cm SSD. The data are of the 10 MV photon beam.

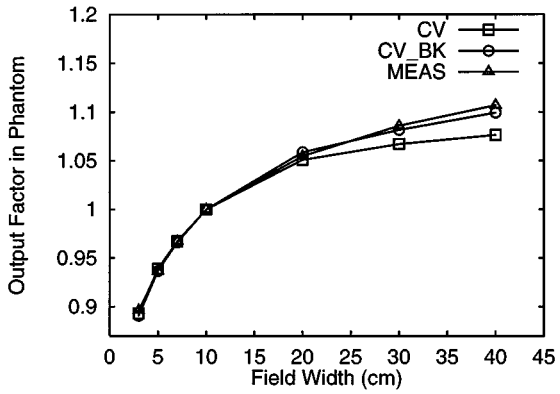

FIG. 11. The total output factors S_{cp} from the convolution calculation (''CV''), the backscatter corrected convolution calculation (''CV_BK''), and the measurement (''MEAS''). The data are of the 10 MV photon beam.

miniphantom. The convolution calculation gives a theoretical prediction of the variation of the S_c factor, because the S_{cb} factor is not phantom dependent in this case.

Figure 9 shows the convolution calculated S_{ca} at 80, 100, and 150 cm SSDs in the fields of $3\times3-40\times40$ cm^2 (defined at SAD) of the 10 MV photon beam. The 10×10 cm^2 field at SAD was used as the reference field. This figure shows that the head scatter factor changes little with the SSD at large field sizes. However, the S_{ca} is reduced about 1% at a shorter SSD in the smaller fields, because of a greater variation of the extra-focal photon fluence from the field of 3×3 cm^2 to the field of 10×10 cm^2. This can be illustrated by Eq. (9), which shows that the projection PS is also a function of phantom location zp. Yet the deviation of S_c at different SSDs is small and could be within the statistical uncertainty of a measurement.

Figure 10 shows the calculated S_{ca} as a function of the calculation depth in the fields of $3\times3-40\times40$ cm^2 at 100 cm SSD. Because the extra-focal photons have lower energies than the primary photons, the relative strength of the extra-focal source decreases with the depth in the phantom. This causes about 1% difference in the S_{ca} in the field of 3×3 cm^2. Yet this deviation is also too small to be distinguished by measurements. Thus an appropriate measurement depth such as 5 cm can be chosen to reduce the electron contamination in the photon fields. In wedged fields, the difference in the attenuation of the primary and the extra-focal photons is magnified. This effect should be accounted for to model the output factor correctly in the wedged field.

F. Total output factors in phantom

Figure 11 shows the S_{cp} factors from the convolution calculation and from the measurement in the fields of $3\times3-40\times40$ cm^2 of the 10 MV photon beam. The data of ''CV'' are directly from the dose calculation. The data of ''CV_BK'' are from the ''CV'' plus the backscatter correction. A good agreement within 1% between the ''CV_BK'' and the ''MEAS'' data are shown by the results.

Figure 12 shows a comparison of the S_{cp} factors (without the backscatter correction), the S_{ca} factors, and the S_p factors from the convolution calculation. The results show that the contribution from the head scatter and the phantom scatter to the total photon output are of a similar magnitude at small fields up to 20×20 cm^2. Beyond this field, the phantom scatter alone causes a continuous increase of the S_{cp} in large fields. Figures 11 and 12 show that the total photon output increase is about 22% from the field of 3×3 cm^2 to the field of 40×40 cm^2. The contribution from the backscattered radiation, the extra-focal radiation, and the phantom scatter are approximately 2%, 9%, and 11%, respectively. The contribution from the phantom scatter can decreases slightly at a higher beam energy, because the scattered radiation tends to be more forward directed along the incident direction of the photon beam, which reduces the lateral phantom scatter at shallow depths.

We have also computed the S_{cp} factors from two alternative approaches. The first one is based on a direct dose calculation, the second one is from a product of the S_{ca} and S_p factors. Figure 12 also shows an excellent agreement be-

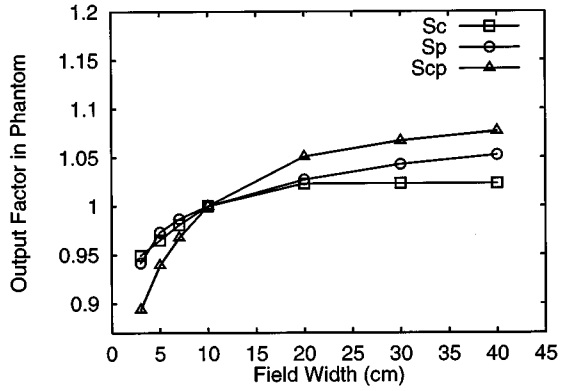

FIG. 12. The head scatter factors (''Sc'' without the backscatter correction), the phantom scatter factors (''Sp''), and the total output factors (''S_{cp}'' without the backscatter correction) from the convolution calculation. The S_{cp} from the direct convolution calculation is shown by the continuous line, the product of the S_c and S_p are shown in discrete data points. The data are of the 10 MV photon beam.

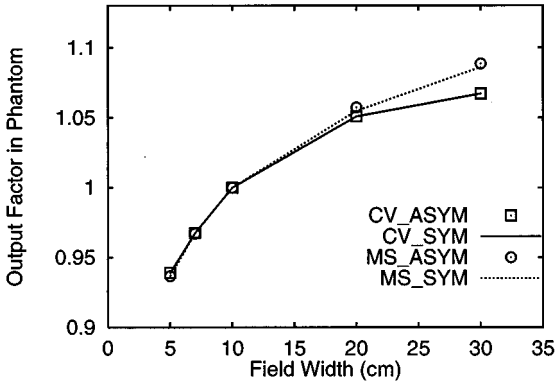

FIG. 13. The total output factors S_{cp} in the asymmetric fields from the convolution calculation (''CV_ASYM,'' without the backscatter correction) and the measurement (''MS_ASYM''). The fields are $3\times3-30\times30$ cm^2, centered at 5 cm off-axis along both x and y directions on the isocenter plane. The S_{cp} in the symmetric fields of the same fields sizes from the convolution calculation (''CV_SYM,'' without the backscatter correction) and the measurement (''MS_SYM'') are also shown for comparison. The data are of the 10 MV photon beam.

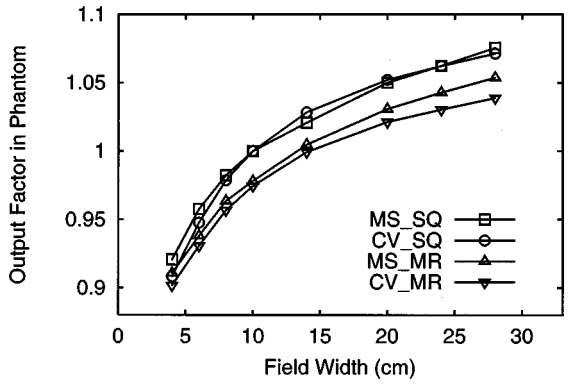

FIG. 14. The total output factors S_{cp} in the MLC defined fields from the convolution calculation and the measurement. The field width is the maximum opening between the opposed leaf ends. ''MS_SQ'' and ''CV_SQ'' are the measured and the calculated data in the square MLC fields, respectively. ''MS_MR'' and ''CV_MR'' are the measured and the calculated data in the mushroom shaped MLC fields, respectively. The data are of the 6 MV photon beam.

tween the results from the two approaches, which indicates that the convolution method can be used to model the phantom scatter more accurately and efficiently. This is because in the convolution algorithm, the scattered dose in the 3D volume can be accounted for intrinsically by using the photon dose kernel. In contrast, it is usually more difficult to estimate the phantom scatter accurately from direct measurements without using specially designed techniques.[2,16]

G. Output factors in asymmetric fields

Figure 13 shows the S_{cp} in $5\times5-30\times30$ cm^2 asymmetric fields of the 10 MV photon beam. The output factors were calculated at the center of the field $(x,y)=(5,5)$ cm, 5 cm deep in the phantom. The asymmetric 10×10 cm^2 field was used as the reference field. This figure shows that the S_{cp} from the convolution method is about 2% lower than the measured data at the 30×30 cm^2 field because the backscatter correction is not included. In comparison, the output factors in symmetric fields of the same field sizes are also shown by the figure. The symmetric reference field of 10×10 cm^2 is used for these data. Both the calculated and the measured results show that the increase of the photon output in the asymmetric fields is of similar magnitude to that in the symmetric fields. Similar observations were reported by other investigators[29–32] as well based on measurements.

From the prospective of the convolution calculation, the total dose at the center of the field depends on the terma or the energy fluence at this point, which is contributed by the primary photon source and the extra-focal photon source. Thus the output factor in air can be modeled as

$$S_{ca}(fs)=\frac{\Psi_p+\Psi_{ef}(fs)}{\Psi_p+\Psi_{ef}(fs0)}=\frac{\Psi_p+ws(fs)\times\Psi_{ef}(\max\ fs)}{\Psi_p+ws(fs0)\times\Psi_{ef}(\max\ fs)},\tag{10}$$

in which Ψ_p and $\Psi_{ef}(fs)$ are the energy fluence of the primary photons and the extra-focal photons, respectively. The $\Psi_{ef}(fs)$ increases with field size, and has the maximum value in the largest field ($\max fs$). The variation of the $\Psi_s(fs)$ with field size can be modeled by a product of the source weighting factor $ws(fs)$ with the $\Psi_s(\max fs)$.

Previously we have demonstrated[10] that the change of the extra-focal photon fluence can be predicted accurately by accounting for the finite source size or the jaw aperture effect on the extra-focal source. More importantly, the increase of the extra-focal photons with field size is not affected by the off-axis position of the field. Thus the output factors expressed by Eq. (10) do not differ from symmetric fields to asymmetric fields, provided that the reference field $fs0$ is chosen correspondingly as a symmetric field or an asymmetric field. Although in reality, there is a slight change of Ψ_p with lateral positions across the field, this variation is usually within a few percent and has little effect on the overall output factors. In addition, our results from the BEAM simulation also showed that the $S_{cb}(fs)$ factor due to the backscattered radiation did not vary significantly from the symmetric fields to the asymmetric fields centered at $(x,y)=(5,5)$ cm. Therefore, the backscatter effect did not cause significant change for the two sets of fields, which has been shown by the measured data as well in Fig. 10.

Typically the symmetric 10×10 cm^2 field is used as the reference field. Thus to obtain the output factors for asymmetric fields, an off-axis dose ratio OAR has to be applied to the output factors measured for symmetric fields. The OAR is defined as the ratio of the dose in the asymmetric reference field $D(fs0\_\text{asym})$ to the dose in the symmetric reference

field $D(fs0\_\text{sym})$, i.e., $D(fs0\_\text{asym})/D(fs0\_\text{sym})$. The OAR factor depends on the change of the total energy fluence with lateral positions. The OAR factor from the convolution calculation was 1.034, which agreed well with the measured data. Previous studies[29,31,32] also showed that the OAR can also be obtained directly from dose profiles measured in the largest open field.

H. Output factors in blocked fields

Figure 14 shows the S_{cp} factors in the fields defined by the MLC from the convolution calculation and the measurement. Results of two types of fields are shown including the square fields and the mushroom shaped fields. The field width is the maximum opening between the opposed leaf ends. The MLC defined 10×10 cm^2 field is used as the reference field. The figure shows that the convolution calculation agrees very well with the measured data within 2% in all the fields. The discrepancies in the mushroom shaped fields could be due to the leakage through the leaves, especially near the rounded leaf edges, which is not accounted for in the convolution calculation at this time. A comparison of the calculated and the measured output factors in other irregular clinical treatment fields have also confirmed a similar level of agreement between the convolution calculation and the measurement. This indicates that the convolution algorithm can be used to accurately compute the output factors in blocked fields such as those defined by the MLC.

The convolution calculation has shown that the total output in the MLC defined reference field is 2% higher than that in the jaw defined reference field (10×10 cm^2). This is because the MLC is further away from the photon sources than the jaws, thus the MLC allows more extra-focal photons to reach the phantom. This follows the same principle as what has been discussed earlier for the jaw exchange effect. In addition, because the jaws were immobilized at a field size 35×35 cm^2 in the MLC defined reference field, while they were 10×10 cm^2 apart in the jaw defined reference field, the backscattered radiation also contributed to the difference in the total output. This has been shown by our measured data that the dose in the MLC defined reference field was 4.3% higher than that in the jaw defined reference field. Thus a reduction of the backscattered radiation from the jaws has to be about 2% to cause the 4.3% increase of the output. This magnitude agrees well with what we have estimated for the effect of the backscattered radiation. For clinical treatments using the MLC, the jaws are usually moved to the manufacturer's recommended positions to minimize the leakage through the leaves. In this case, the backscattered radiation should be taken into account to calculate the output factors for the MLC defined fields.

IV. FURTHER DISCUSSION

The above results demonstrate that the dual source photon beam model, which is based on the Monte Carlo simulation of linear accelerators, represents the intrinsic characteristics of clinical photon beams. Our convolution algorithm using this new photon beam model can predict the photon output accurately for arbitrary treatment fields defined either by the jaws or a secondary field shaper such as the MLC. The most important aspects in calculating the photon output are the correct modeling of the extra-focal source and the backscattered radiation. Our approach is relatively simpler and more efficient than those proposed previously for the similar convolution methods[7,9] provided that the extra-focal source can be accurately described.

In this study, the head structure and the component modules used in simulating the linear accelerator were simplified from those in constructing a realistic machine. For example, the jaws and the MLC were treated as simple apertures in the convolution method, although a more complicated model could be used to account for the physical geometry more accurately. Also, the photon beam characterization was derived from the phase space data based on certain assumptions and approximations. For example, to improve the calculation efficiency, a single extra-focal source was used to generalize all the scattered photons from the head of the machine. Therefore, small discrepancies could exist between the calculated and the measured output factors. A more sophisticated model could improve the calculation accuracy by a marginal extent, but may be less favorable in clinical practice, because of the trade-off between the accuracy and the efficiency of the dose calculation. This is particularly true for a model based dose calculation method such as the convolution approach. A simple and elegant method such as the one proposed here, could be more appropriate for clinical applications, such as in calculating monitor units for patient treatments.

V. SUMMARY

The majority of the photons generated by a linear accelerator are the primary photons directly from the target. The flattening filter and the primary collimator are two major components where the extra-focal photons are created. The number of the extra-focal photons increases with jaw opening. Thus the total photon energy fluence at the isocenter increases by about 8% from 3×3 cm^2 to 40×40 cm^2 of the 10 MV photon beam. This increase occurs mostly in smaller fields because the extra-focal source is partially blocked by the jaws (below 20×20 cm^2). The effect of the finite size of the extra-focal source can be modeled based on a convolution of the source distribution with the collimator aperture function. This approach can be used to accurately predict the variation of the extra-focal radiation in different treatment fields.

The scored dose in the monitor chamber from the backscattered radiation also decreases with the jaw opening. This causes an increase of the photon output by 2%–3% in the largest field (for the kapton chamber). A correction for the backscattered radiation can be combined with the convolution calculation to calculate realistic output factors comparable to the measured data. Our results show that the total photon output in phantom increases by 22% from 3×3 cm^2 to 40×40 cm^2 of the 10 MV photon beam. This is due to an

increase of the head scatter and the phantom scatter by 11% and 10%, respectively.

Both the extra-focal photon fluence and the backscattered radiation to the monitor chamber depend on the field geometry, such as the locations of the source, the collimators, and the phantom. This causes a difference in photon output for fields defined by different collimators. Our results show that the jaw exchange effect and the output in the fields defined by the MLC can be modeled accurately when a realistic beam geometry is used in the convolution method. The output factor also changes slightly with the SSD of the phantom or the depth in the phantom. This effect has been indicated by the convolution calculation, yet it is not clinically significant. The increase of the extra-focal radiation with field size does not vary from symmetric fields to asymmetric fields. This is because the effect of the extra-focal photons does not depend on the location of the field, but rather on the size of the field. This has been shown by both the convolution calculation and the measurement.

Our results have demonstrated that our convolution dose calculation algorithm, which relies on the intrinsic characteristics of clinical photon beams, can be used to predict the photon output and thus to calculate monitor units for clinical treatments in an accurate and efficient fashion.

ACKNOWLEDGMENTS

This work is partly funded by a research fellowship from Mayo Clinic and Foundation. The convolution/superposition program was originally developed under the NCI Grant No. CA 48902. The BEAM code was developed under the NCI Grant No. CA52692. We would like to thank our colleagues in the National Research Council of Canada, and in the Department of Medical Physics, University of Wisconsin at Madison in developing the BEAM code, particularly Dr. Dave Rogers, Dr. Charlie Ma, Daryoush Sheikh-Bagheri, and Dr. James Yang. We appreciate the communication with Dr. Michael Sharpe of the William Beaumont Hospital, MI. We also thank Varian Corporation in providing the original treatment machine data used for the Monte Carlo simulation.

[a]Electronic-mail: mackie@macc.wisc.edu

[1]K. R. Kase and G. K. Svensson, ''Head scatter data for several linear accelerators (4–18 MV),'' Med. Phys. **13**, 530–532 (1986).
[2]G. Luxton and M. A. Astrahan, ''Output factor constituents of a high-energy photon beam,'' Med. Phys. **15**, 88–91 (1987).
[3]P. B. Dunscombe and J. M. Nieminen, ''On the field-size dependence of relative output from a linear accelerator,'' Med. Phys. **19**, 1441–1444 (1992).
[4]D. A. Jaffray and J. J. Battista, ''X-ray sources of medical linear accelerators: Focal and extra-focal radiation,'' Med. Phys. **20**, 1417–1427 (1993).
[5]E. L. Chaney and T. J. Cullip, ''A Monte Carlo study of accelerator head scatter,'' Med. Phys. **21**, 1383–1390 (1994).
[6]T. C. Zhu and B. E. Bjärngard, ''The head-scatter factor for small field sizes,'' Med. Phys. **21**, 65–68 (1994).
[7]M. B. Sharpe, D. A. Jaffray, J. J. Battista, and P. Munro, ''Extrafocal radiation: A unified approach to the prediction of beam penumbra and output factors for megavoltage x-ray beams,'' Med. Phys. **22**, 2065–2074 (1995).
[8]F. Z. Khan, W. Sewchand, J. Lee, and J. F. Williamson, ''Revision of tissue-maximum ratio and scatter-maximum reaction concepts for cobalt 60 and higher energy x-ray beams,'' Med. Phys. **7**, 230–237 (1980).
[9]A. Ahnesjö, ''Application of the convolution method for calculation of output factors for therapy photon beams,'' Med. Phys. **19**, 295–301 (1992).
[10]H. H. Liu, T. R. Mackie, and E. C. McCullough, ''A dual source photon beam model used in convolution/superposition dose calculations for clinical megavoltage x-ray beams,'' Med. Phys. **24**, 1960–1974 (1997).
[11]T. R. Mackie, A. Ahnesjö, P. Dickof, and A. Snider, ''Development of a convolution/superposition method for photon beams,'' in *Proceedings of the 9th International Conference on Computers in Radiotherapy*, Den Haag, Amsterdam (Elsevier Science, Amsterdam, 1987), pp. 107–110.
[12]A. Ahnesjö, ''Collapsed cone convolution of radiant energy for photon dose calculation in heterogeneous media,'' Med. Phys. **16**, 577–592 (1989).
[13]T. R. Mackie, P. J. Reckwerdt, M. A. Gehring, T. W. Holmes, S. S. Kubsad, B. R. Thomadsen, C. A. Sanders, B. Paliwal, and T. J. Kinsella, ''Clinical Implementation of the convolution/superposition method,'' in *Proceedings of the 10th International Conference on Computers in Radiotherapy*, Lucknow, India (Alpana Arts, Lucknow, India, 1990), pp. 322–325.
[14]A. Ahnesjö, ''A pencil beam model for photon dose calculation,'' Med. Phys. **19**, 263–273 (1992).
[15]D. W. O. Rogers, B. A. Faddegon, G. X. Ding, C. M. Ma, J. We, and T. R. Mackie, ''BEAM: A Monte Carlo code to simulate radiotherapy treatment units,'' Med. Phys. **22**, 503–524 (1995).
[16]J. M. van Gasteren, S. Heukelom, H. J. van Kleffens, R. van der Laarse, J. L. M. Venselaar, and C. F. Westermann, ''The determination of phantom and collimator scatter components of the output of megavoltage photon beams: measurement of the collimator scatter part with a beam-coaxial narrow cylindrical phantom,'' Radiother. Oncol. **20**, 250–257 (1991).
[17]R. Mohan and C. Chui, ''Use of fast Fourier transforms in calculating dose distributions for irregularly shaped fields for three-dimensional treatment planning,'' Med. Phys. **14**, 70–77 (1987).
[18]G. Starkschall, ''A convolution method for constructing primary beam profiles in the presence of beam modifiers,'' Med. Phys. **15**, 657–661 (1988).
[19]M. K. Yu, R. S. Sloboda, and F. Mansour, ''Measurement of photon beam backscatter from collimators to the beam monitor chamber using target-current-pulse-counting and telescope techniques,'' Phys. Med. Biol. **41**, 1107–1117 (1996).
[20]D. L. Watts and G. S. Ibbott, ''Measurement of beam current and evaluation of scatter production in an 18-MeV accelerator,'' Med. Phys. **14**, 662–664 (1987).
[21]P. Huang, J. Chu, and B. E. Bjärngard, ''The effect of collimator backscatter radiation on photon output of linear accelerators,'' Med. Phys. **14**, 268–269 (1987).
[22]H. Kubo, ''Telescopic measurements of backscattered radiation from secondary collimator jaws to a beam monitor chamber using a pair of slits,'' Med. Phys. **16**, 295–298 (1989).
[23]C. Duzenli, B. McClean, and C. Field, ''Backscatter into the beam monitor chamber: Implications for dosimetry of asymmetric collimators,'' Med. Phys. **20**, 363–383 (1993).
[24]P. D. Higgins, W. H. Sohn, C. H. Sibata, and W. A. McCarthy, ''Scatter factor corrections for elongated fields,'' Med. Phys. **16**, 800–802 (1989).
[25]M. Tatcher and B. Bjärngard, ''Head-scatter factors in rectangular photon fields,'' Med. Phys. **20**, 205–206 (1993).
[26]M. K. Yu, B. Murray, and R. Sloboda, ''Parameterization of head-scatter factors for rectangular photon fields using an equivalent square formalism,'' Med. Phys. **22**, 1329–1332 (1995).
[27]J. A. Meli, ''Output factors and dose calculations for blocked x-ray fields,'' Med. Phys. **13**, 405–408 (1986).
[28]E. M. Dean and J. B. Davis, ''Output factors for blocked fields,'' Br. J. Radiol. **66**, 517–522 (1993).
[29]F. M. Khan, B. J. Berbi, and F. C. Deibel, ''Dosimetry of asymmetric x-ray collimators,'' Med. Phys. **13**, 936–941 (1986).
[30]J. R. Palta, K. Ayyangar, and N. Suntharalingam, ''Dosimetric characteristics of a 6 MV photon beam from a linear accelerator *x* with asymmetric collimator jaws,'' Int. J. Radiat. Oncol., Biol., Phys. **14**, 383–387 (1988).
[31]M. Tenhunen and T. Lahtinen, ''Relative output factors of asymmetric megavoltage beams,'' Radiother. Oncol. **32**, 226–231 (1994).
[32]B. Murray, B. McClean, and C. Field, ''Output factors for fields defined by four independent collimators,'' Med. Phys. **22**, 285–290 (1994).